Consequences of Nonergodicity in Aqueous Binary PEO−PB Micellar Dispersions

Sumeet Jain and Frank S. Bates*

Department of Chemical Engineering and Materials Science, University of Minnesota, Minneapolis, Minnesota 55455

Received September 29, 2003; Revised Manuscript Received December 10, 2003

ABSTRACT: Aqueous micellar dispersions of poly(ethylene oxide)−poly(butadiene) (PEO−PB) diblock copolymers were investigated using cryogenic transmission electron microscopy (cryo-TEM). A variety of binary blends were prepared by premixing (before dispersion) and postmixing (after dispersion) diblocks with varying composition and molecular weight. Cryo-TEM results establish there is no perceptible exchange of macromolecules between aggregates resulting in a nonergodic state, where overall equilibrium is never achieved. However, analysis of many microscopic images leads to the conclusion that these nonergodic micelles relax to a state of local equilibrium through the redistribution of block copolymers within the topological framework established during dispersion. Different average compositions and molecular weights exhibit varying degrees of structural complexity, which appears to peak in the vicinity of network formation. Away from this condition the micelle morphology is relatively insensitive to core or corona polydispersity. However, at compositions where the monomodal and nearly monodisperse amphiphiles produce branched wormlike micelles and a network, bimodal mixtures displayed intramicellar segregation leading to cylindrical undulations and octopus-like aggregates with cylindrical micelles emanating from a single bilayer core. These findings are discussed in the context of interfacial curvature and surfactancy.

Introduction

Surfactant mixtures often are substituted for pure surfactants in commercial applications such as detergency and cosmetics. Mixtures of amphiphiles offer attractive advantageous over single component formulations in achieving specific properties. Living tissue provides an elegant example where cell membranes are constructed from as many as 10 different types of lipids. Moreover, the purification of surfactants can be costly and difficult. An expansive experimental knowledge of surfactant mixtures including the critical micelle concentration (cmc) and micelle shapes and dimensions as a function of composition has been established.[1] However, a fundamental molecular level understanding of surfactant mixture phase behavior remains somewhat elusive.

Amphiphilic diblock copolymers are macromolecular analogues of conventional surfactants and lipids. Slow chain dynamics and large chain lengths are two factors that complicate micellization of these macromolecular surfactants. As with the low molecular weight analogues, precise tailoring of molecular weight and composition offers control over the morphological behavior of polymeric dispersions. However, because of synthetic limitations, targeting exact molecular weights and compositions can be difficult. An alternative method for controlling morphology is mixing of two or more diblock copolymers, a technique employed successfully with undiluted block copolymer melts.[2−4] Relatively little is known about the aggregation behavior of aqueous solutions of amphiphilic diblock copolymer mixtures.[5] In this report, we expand on earlier studies[6,7] that dealt with aqueous dispersions of monomodal and relatively monodisperse diblock copolymers. Here we examine the consequences of increasing molecular weight, and binary blending, on the structure and stability of dispersed micelles, using cryogenic transmission electron microscopy (cryo-TEM) as the principal experimental tool.

The aggregation behavior of dispersions of diblock copolymers is more complicated than that of low molecular weight surfactants. Many attempts have been made to understand the kinetics and mechanisms of chain exchange between diblock copolymer micelles using a wide range of experimental techniques[8] such as fluorescence nonradiative energy transfer,[9−11] temperature-jump measurements,[12,13] time-resolved light scattering,[14,15] and pulsed-field gradient NMR.[16] These studies mostly focused on marginal amphiphilic systems displaying fast micelle dynamics (e.g., the Pluronics[8]). Highly amphiphilic systems involving diblock copolymers and polar solvents such as water have not been extensively probed for micelle dynamics.[6,17] Component exchange in polymeric systems should be extremely slow due to a low critical micelle concentration (cmc), which nearly eliminates the presence of free chains in solution. Most kinetic studies involving amphiphilic block copolymers have been conducted with glassy micelle cores, e.g., poly(styrene)[18,19] and poly(methyl methacrylate).[20] In these systems, the slow dynamics most likely originates from the vitrified nature of the core-forming block. Dormidontova[21] proposed a "micelle fusion/fission−unimer exchange" mechanism for block copolymer micelle evolution, suggesting that micelle fusion/fission dominates the kinetics over unimer exchange. These predictions were contrary to the Aniansson−Wall[22,23] mechanism for surfactant micelles. Rager et al.[20] reported that the micelle−unimer equilibrium in diblock copolymer micelles is governed by the thermodynamics of aggregation rather than a kinetic hindrance. Creutz et al.[17] reported that the exchange of chains between block copolymer aggregates is 10^{-9}−10^{-11} times slower than in surfactant micelles. Relatively few studies have addressed the issue of micelle dynamics in unencumbered (i.e., liquid core) systems such as those containing poly(isoprene)[24] or poly(butadiene).[6,25]

10.1021/ma035467j CCC: $27.50
Published on Web 01/30/2004

Slow chain exchange implies that polymeric micelles do not interact, thus forming a nonergodic (i.e., locally isolated) array of aggregates. This notion has been hypothesized for some time[6,26] but not demonstrated conclusively. Absence of molecular exchange was established by Won et al.[6] in mixtures of normal and partially deuterated PEO−PB using small-angle neutron scattering measurements. Both spherical and wormlike micelles failed to exchange polymers after a week in aqueous solution. In this report we provide real-space cryo-TEM images that directly evidence the consequences of slow polymer micelle dynamics. An important conclusion of this study is that dispersed morphologies are kinetically trapped after evolution.

Another important parameter that is often implicated in rationalizing complications associated with diblock copolymer dispersions is block length polydispersity. Phenomena such as coexisting morphologies are believed to occur as a consequence of the polydispersity in chain lengths, which allows the polymer chains to assemble in more than one aggregate geometry. Some theoretical efforts[27,28] have addressed the effect of polydispersity on the cmc and micellar size and aggregation number. Few experimental studies[29] have been devoted to understanding the effect of polydispersity on diblock copolymer self-assembly. The aggregate morphology assumed by an amphiphile results from a balance of three contributions to the free energy: chain stretching in the core, the interfacial energy, and the repulsion between coronal chains.[30] In certain regions of the parameter space governed by composition and molecular weight, this balance of forces appears to be more subtle than in others. The formation of Y-junctions and network structures seems to occur in a narrow region above a critical molecular weight.[7] By analogy with network formation in bulk block copolymers (e.g., the gyroid morphology), the associated saddle surfaces at the water−hydrocarbon interface likely represents a compromise between the cylindrical and bilayer (vesicle) structural elements. We have examined the role of polydispersity in this and other regions of the space defined by average diblock copolymer composition and molecular weight through binary blending.

For the kinetic study, blends of two diblock copolymers were prepared in two different ways: by mixing two polymers before (premixing) and after (postmixed) dissolution in water. The morphological behavior of such dispersions was then documented using cryo-TEM. To investigate the effect of polydispersity, relatively monodisperse diblock copolymers were premixed to artificially broaden the molecular weight distribution. Pairs of diblock copolymers were blended to systematically map the morphology diagram for identical and different core molecular weights. Results obtained from cryo-TEM provide a unique glimpse into the consequences of blending and the role of polydispersity in different regions of the morphological diagram.

Experimental Section

Materials. For the present study, two series of poly(ethylene oxide)−poly(butadiene) (OB) block copolymers were synthesized by anionic polymerization,[31] each characterized by a constant core molecular weight. 1,3-Butadiene (Aldrich) was anionically polymerized using *sec*-butyl-lithium initiator in tetrahydrofuran (THF), thereby forming poly(1,2-butadiene) (PB). A large batch (∼120 g) of living PB was end-functionalized by addition of ethylene oxide followed by termination with acidic methanol. Aliquots of this hydroxylated polymer were reinitiated in THF using potassium naphthalenide and then reacted with defined amounts of ethylene oxide and terminated with acidic methanol to form the OB block copolymers. For each series, different length segments of hydrophilic (O) blocks were added in order to achieve a varying degree of amphiphilicity in the diblock copolymers. This two-step synthesis scheme is specifically advantageous in this study as it yields different diblock copolymers derived from a single core (B) block. Polydispersity indices (PDI) were determined by gel permeation chromatography (GPC) using a Waters 150C instrument fitted with Phenogel columns and calibrated with poly(styrene) standards (Pressure Chemical Co.). Proton (^{1}H) NMR spectroscopy was used to determine the PB microstructure (i.e., 90% 1,2 addition). The weight fractions of PEO (w_{PEO}) and the number-average molecular weights (M_n) were estimated from the reaction stoichiometry and confirmed by ^{1}H NMR measurements. For the OB1 series, 14 different diblock copolymers were synthesized with a core molecular weight of 2.5 kg/mol (degree of polymerization, N_{PB} = 46) and PEO weight fractions ranging from 0.30 to 0.64 (1.03 < PDI < 1.06). The second group of 13 different diblock copolymers (OB9 series) was synthesized with a core molecular weight of 9.2 kg/mol (N_{PB} = 170) and PEO weight fractions ranging from 0.24 to 0.70 (1.04 < PDI < 1.10). A complete listing of these compounds is provided in Table 1. In the present study, the material chosen for the hydrophobic core is 1,2-polybutadiene, having a glass transition temperature of −12 °C.[32]

Table 1. Molecular Characteristics of Block Copolymers[a]

ID[b]	M_n (kg/mol)[c]	N_{PB}[d]	N_{PEO}[e]	w_{PEO}[f]	PDI[g]	micelle structure[h]
OB1-1	4.4	46	44	0.43	1.04	C, B
OB1-2	3.5	46	28	0.32	1.05	B
OB1-3*	5.2	46	58	0.50	1.05	C, S
OB1-4*	7.6	46	103	0.64	1.04	S
OB1-5*	4.3	46	42	0.42	1.04	B, C
OB1-6	5.8	46	69	0.54	1.03	C, S
OB1-7	7.0	46	93	0.62	1.04	S, C
OB1-8	5.0	46	56	0.49	1.03	C
OB1-9	3.9	46	35	0.37	1.04	B, C
OB1-10	3.7	46	30	0.34	1.06	B
OB1-11	3.4	46	24	0.30	1.03	B
OB1-13	5.4	46	63	0.52	1.04	C
OB1-14	5.3	46	60	0.51	1.04	C
OB1-15	4.1	46	39	0.40	1.04	B, C
OB9-1*	15.8	170	150	0.42	1.04	C
OB9-2	16.4	170	164	0.44	1.05	C, S
OB9-3	19.0	170	225	0.51	1.06	S, C
OB9-4*	14.0	170	110	0.34	1.04	N
OB9-5*	18.1	170	203	0.49	1.05	S,C
OB9-6*	12.1	170	66	0.24	1.04	B
OB9-7	19.3	170	231	0.52	1.04	S, C
OB9-9	16.1	170	158	0.43	1.04	C, S
OB9-10	16.0	170	156	0.43	1.10	C, S
OB9-11*	15.1	170	134	0.39	1.04	C_Y
OB9-12*	30.2	170	478	0.70	1.09	S
OB9-13	24.2	170	341	0.62	1.08	S
OB9-15*	13.2	170	90	0.30	1.06	B, C_Y

[a] Diblock copolymers used in this study are indicated by an asterisk. [b] Diblock copolymers of poly(ethylene oxide) (PEO) and poly(butadiene) (PB). [c] Number-average molecular weight determined from reaction stoichiometry and ^{1}H NMR. [d] Number of monomer repeat units in PB block. [e] Number of monomer repeat units in PEO block. [f] Weight fraction of PEO block in diblock copolymer. [g] Polydispersity index determined from gel permeation chromatography. [h] Aggregation morphologies formed in water identified with cryo-TEM: B = bilayers; C = cylinders, S = spheres, N = network, C_Y = cylinders with Y-junctions. Coexisting structures are written in order of statistical predominance.

Cryogenic Transmission Electron Microscopy. Sample solutions for analysis by cryo-TEM were prepared by dissolution of block copolymer in deionized, double-distilled water (Corning Mega-Pure System) at a concentration of 1 wt %. Direct dissolution is the simplest technique for sample preparation and hence was preferred over other techniques such as dialysis.[33] After addition of water, the samples were sealed

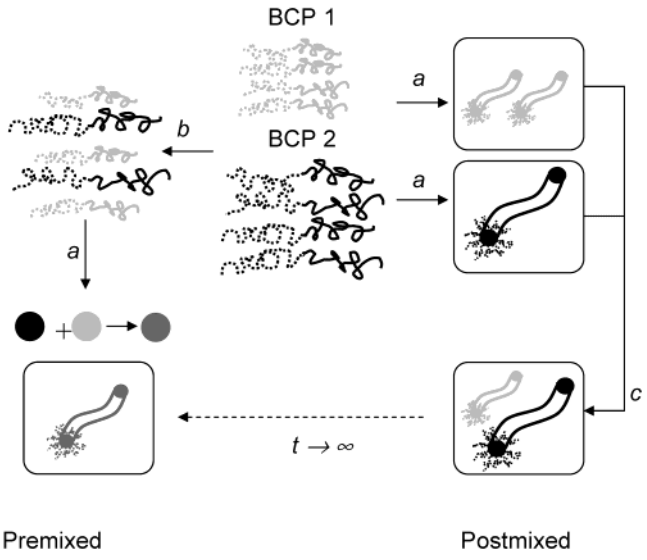

Figure 1. Schematic illustrating the two mixing protocols: premixing and postmixing. For premixing, block copolymer 1 (BCP1) and block copolymer 2 (BCP2) are dissolved in methylene chloride, a good solvent, followed by drying and annealing of the blend at 45 °C (step b). The dried mixture is then hydrated with water (1 wt %) (step a), and the morphologies are analyzed using cryo-TEM. For postmixed blends, block copolymers (BCP1 and BCP2) are first individually dissolved in water (1 wt %) (step a), and then predetermined amounts of block copolymer solutions are mixed (step c), followed by analysis using cryo-TEM. Given infinite time the postmixed solution should equilibrate to the same thermodynamic state as the premixed sample.

and stirred at room temperature for minimum of 2 weeks. Most polymers dispersed in water in a few hours except the ones with high hydrophobic content, which took several days. In all cases described here the solutions appeared homogeneous to the naked eye although they were characterized by varying degrees of opacity.

Vitreous samples for morphological studies were prepared in a custom-built special chamber referred to as the controlled-environment vitrification system (CEVS).[34] To prevent any loss of water from sample solution, the CEVS chamber was humidified to saturation at 25 ± 0.2 °C. Vitreous samples were prepared by pipeting a drop (∼5 μL) of polymeric solution onto a cryo-TEM grid, held by tweezers. Excess solution was blotted by a piece of filter paper, resulting in the formation of thin film about 100−300 nm thick held by capillary forces within the holes of a lacey carbon film supported on the metal grid. After blotting, the samples were allowed to equilibrate for a minimum of 30 s to relax any residual stresses. The samples were then quickly plunged into a reservoir of liquid ethane cooled by liquid nitrogen. Vitrified specimens were mounted on a cryogenic sample holder (Gatan 626) and examined with a JEOL 1210 TEM operated at 120 kV. A minimal dose system was employed to avoid sample damage by radiolysis.[35] Adequate phase contrast was obtained at a nominal underfocus of 3−12 μm. Images were recorded on a Gatan 724 multiscan digital camera and processed with DigitalMicrographs version 3.3.1. The ramp-shaped optical density gradients in the background due to varying sample thickness were digitally corrected. Diffraction grating replicas (Ted-Pella) containing 2160 lines/mm were used to calibrate the microscope.

Blend Mixing Protocols. Sample solutions for analysis using cryo-TEM were prepared in two different ways—mixing dry bulk copolymers before dissolution (premixing) and after dissolution (postmixing) in water (Figure 1). For premixed samples, calculated amounts of diblock copolymers were homogeneously dissolved in methylene chloride, dried, and annealed in a vacuum oven at 45 °C for about 12 h. The dried mixture was then dissolved in deionized, double-distilled water to form a 1 wt % solution. The postmixed samples were prepared by pouring together predetermined amounts of two diblock copolymer solutions and stirring the resulting mixture for a few days. A summary of the binary blends investigated is provided in Table 2.

Table 2. Molar Mixing Ratios for Block Copolymer Pairs

category	BCP 1[a]	BCP 2[b]	x_1[c]	$\langle N_{PB}\rangle$[d]	$\langle w_{PEO}\rangle$[e]	PDI_{PB}[f]	PDI_{PEO}[g]
A	OB9-4	OB9-12	0.50	170	0.58	1.00	1.39
A	OB9-4	OB9-12	0.67	170	0.52	1.00	1.56
A	OB9-4	OB9-12	0.87	170	0.43	1.00	1.61
A	OB9-4	OB9-5	0.50	170	0.43	1.00	1.09
B	OB9-4	OB1-5	0.50	108.5	0.38	1.32	1.20
B	OB9-4	OB1-3	0.50	108.5	0.39	1.32	1.10
B	OB9-4	OB1-4	0.50	108.5	0.45	1.32	1.00
B	OB9-1	OB1-3	0.50	108.5	0.44	1.32	1.20
B	OB9-1	OB1-5	0.50	108.5	0.42	1.32	1.32
C	OB9-1	OB9-6	0.50	170	0.34	1.00	1.15
C	OB9-11	OB9-15	0.50	170	0.34	1.00	1.04
C	OB9-1	OB9-6	0.67	170	0.37	1.00	1.10

[a] Block copolymer 1 in the blend. [b] Block copolymer 2 in the blend. [c] Mole fraction of block copolymer 1 in the blend. [d] Average number of butadiene repeat units in each polymer in the blend. [e] Average weight fraction of PEO chains in the blend. [f] Polydispersity in PB block lengths in the blend assuming the starting copolymers have monodisperse PB blocks. [g] Polydispersity in PEO block lengths in the blend assuming the starting copolymers have monodisperse PEO blocks.

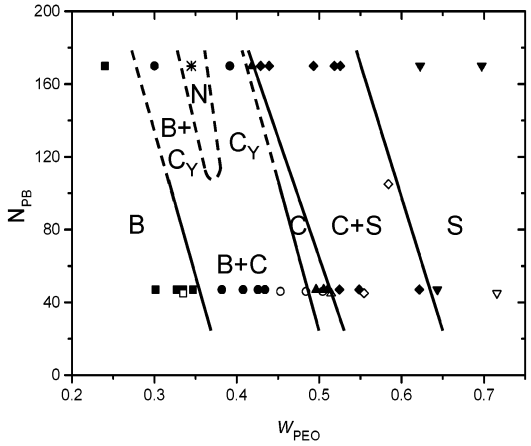

Figure 2. Morphology diagram correlating aggregate structure of PB−PEO micelles in water as a function of the molecular composition. N_{PB} is the degree of polymerization of the PB block, and w_{PEO} is the weight fraction of PEO in the copolymer. The aggregate morphologies were determined using cryo-TEM. The four main geometries are bilayered vesicles (B), network (N), cylinders (C), and spheres (S). Regions of coexistent morphologies are documented for compositions between the B, N, C, and S morphologies. C_Y represents cylinders with occasional Y-junctions. The morphological boundaries do not denote exact transition conditions. Open and filled symbols indicate previous[36] and current experimental results, respectively.

Results

Overview. A well-defined pattern of dispersed morphologies was identified for the OB diblock copolymers in aqueous solution using cryo-TEM. These results are summarized in Figure 2. For series I (N_{PB} = 46), micellar morphologies similar to those reported for conventional surfactants were identified. As the hydrophilic content (w_{PEO}) increased, a familiar sequence of structural elements was documented beginning with bilayers (B) (in the form of vesicles), then cylinders (C), and then spheres (S) separated by composition windows containing mixed morphologies, B + C and C + S. These results are in agreement with earlier reports.[36,37] Such

transitions are well-established on the basis of molecular packing considerations;[38] that is, increasing the hydrophilic block length induces greater interfacial curvature. A balance between interfacial tension and chain stretching while respecting the incompressibility of the core domain leads to an equilibrium domain morphology and size.

Increasing the core molecular weight leads to an additional structural element, cylindrical branches, denoted C_Y, between the B and C regions.[7] The concentration of branches, also referred to as Y-junctions, peaks midway between the C and B regions leading to network (N) formation and necessarily macroscopic phase separation at low diblock copolymer loadings (here 1 wt %). This new morphological state, and the myriad network fragments that result from vigorous agitation, were described in a recent report[7] and motivated much of the work reported here.

Relatively monodisperse, monomodal diblock copolymers identified in Figure 2 were blended with each other following the two mixing protocols described above. Binary blends were prepared by mixing diblock copolymers in three categories: (A) having identical core molecular weights, (B) with different core molecular weights, and (C) having identical core molecular weights around the network composition. Figure 3 illustrates the targeted blends in each of these categories. Cryo-TEM images, obtained from these mixtures, are presented in the remainder of this section. To facilitate this presentation, we split the results into two groups representing mixtures outside and around the network (N) forming region, associated with PEO composition, w_{PEO}*.

Effect of Mixing Protocol. Many studies have explored the micellization of diblock copolymers, but much less attention has been paid to the kinetic aspects of micelle formation. This deficiency can be attributed to a lack of experimental techniques to access exchange kinetics under equilibrium conditions.[26] We studied mixtures of nearly monodisperse diblock copolymers using different mixing protocols in order to assess the equilibration or lack of equilibration of micellar morphologies. The results from two such pairs, OB9-1/OB1-3 and OB9-4/OB9-12, are shown here. The molecular characteristics of these diblock copolymers, and the micelle morphologies as determined by cryo-TEM, are listed in Table 1. The mixing ratios for the blends are documented in Table 2. Only a few representative images drawn from an extensive library of cryo-TEM pictures are presented here.

Parts A and B of Figure 4 contain representative cryo-TEM micrographs of postmixed and premixed samples of OB9-1/OB1-3 (category B, Figure 3B), respectively. Clearly, the two images exhibit qualitatively different morphologies despite having an identical chemical composition. Both diblock copolymers in this pair individually form mainly cylindrical micelles along with some spherical micelles; the cylinder micelles formed by OB9-1 exhibit occasional Y-junctions. The postmixed image (Figure 4A) is characterized by micellar morphologies that represent a superposition of the individual diblock copolymer solutions. The disparity in micelle diameters results from the difference in core block lengths of the constituent diblock copolymers. In the premixed solution (Figure 4B) predominantly spherical micelles coexist with a few short cylinders, each governed by an intermediate diameter which is distinct

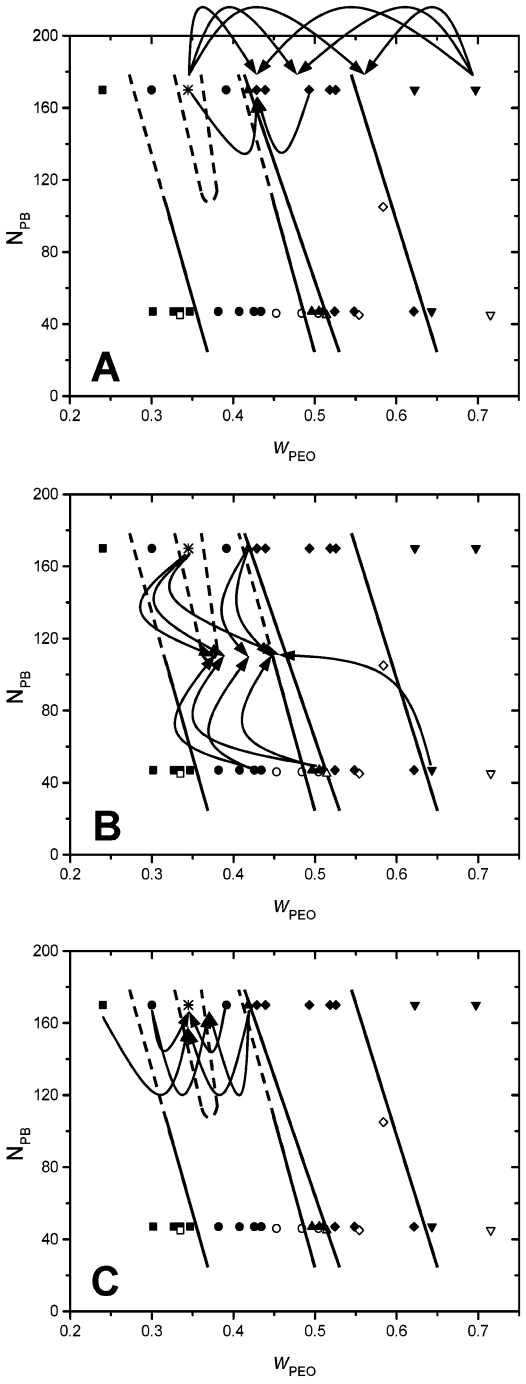

Figure 3. Blending strategies employed in this project. (A) Mixing diblock copolymers with identical core block molecular weights. (B) Mixing diblock copolymers having different core and corona block molecular weights. (C) Mixing around the network composition w_{PEO}* at constant core molecular weight.

from those of the constituent diblock copolymers. Measurements of numerous premixed micelles reveal cylinders with a diameter of about 26 nm (compared to 14 nm for OB1 and 34 nm for OB9) and spheres with an average diameter of 39 nm (compared to 19 nm for OB1 and 46 nm for OB9) (see Table 3). We return to this issue in the Discussion section.

Another set of images obtained from the pair of diblock copolymers OB9-4/OB9-12 containing a common core block (category A, Figure 3A) is shown in Figure 5. Figure 5A illustrates the coexistence of small network fragments with spherical micelles, which are representative of the constituent OB9-4 and OB9-12 solutions.

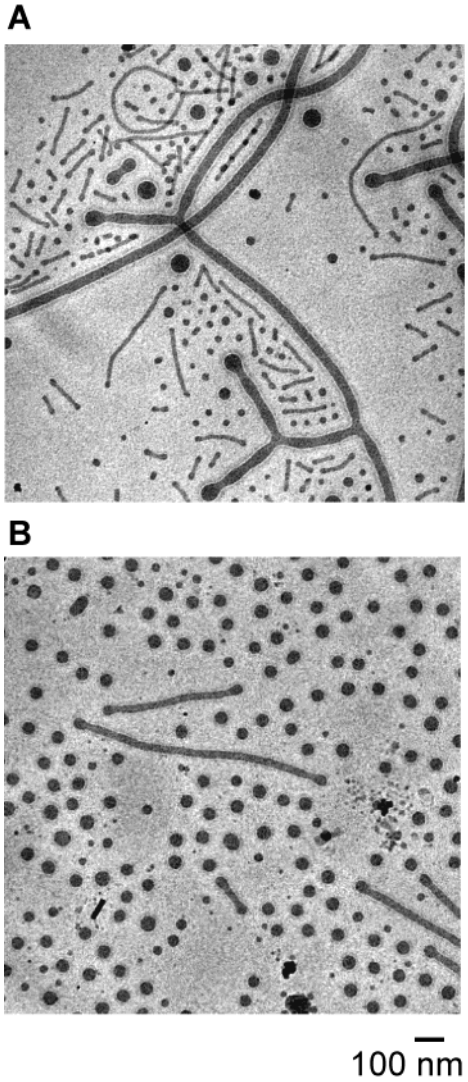

Figure 4. Cryo-TEM images obtained from postmixed (A) and premixed (B) samples of the OB9-1/OB1-3 blend. This comparison illustrates the nonergodic nature of polymeric micelles formed from diblock copolymers with different molecular weights. The small and large micelles in (A) failed to mix after several months.

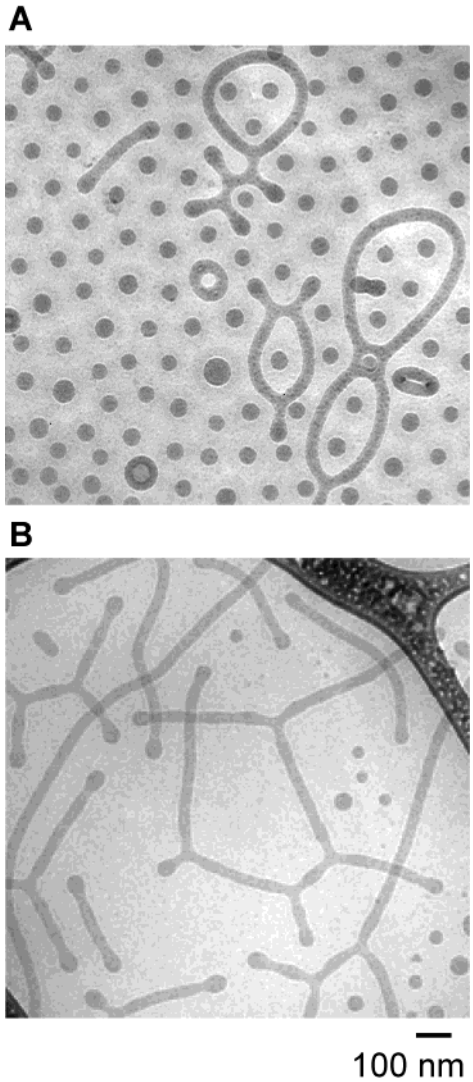

Figure 5. Cryo-TEM images from postmixed (A) and premixed (B) samples of OB9-4/OB9-12 (2:1) blend illustrating nonergodicity of polymeric micelles with identical core molecular weight polymers.

Table 3. Micellar Dimensions of Various Morphologies

morphology	M_n^{core} (g/mol)[a]	d (nm)[b]
spheres	2500 ± 40	$18._4 \pm 2._6$
	9200 ± 200	$46._3 \pm 7._0$
	5850 ± 204	$38._8 \pm 10._2$
cylinders	2500 ± 40	$14._3 \pm 1._6$
	9200 ± 200	$34._2 \pm 2._0$
	5850 ± 204	$25._4 \pm 3._3$
bilayers	2500 ± 40	$8._7 \pm 1._2$
	9200 ± 200	$21._4 \pm 1._9$
	5850 ± 204	$15._8 \pm 2._8$

[a] Error in core molecular weight is obtained from gel permeation chromatography (equipped with light scattering device) analysis. [b] Micellar dimension, d, for sphere and cylinder is the diameter and for bilayer is the wall thickness.

The core dimensions of these micelles are identical to those determined for the neat copolymer solutions (not shown for brevity). However, premixed solutions of OB9-4/OB9-12 self-assemble into long cylindrical micelles with frequently placed Y-junctions along with a few spherical micelles, an intermediate morphology that is roughly consistent with the single-component behavior at a comparable average composition $\langle w_{PEO} \rangle = 0.52$ (see Figure 2). Also, a cylinder diameter of about 34 nm is virtually identical to the monomodal value, which is consistent with the fact that these two diblock copolymers share a common parent core block.

These results illustrate three important blending variables: the method of blending, the average core molecular weight of the blend, and the average composition of the blend. In the following section, we restrict our attention to premixed blends in assessing the morphology diagram in greater detail. These results are presented in two groups: mixtures near the network condition (w_{PEO}*) and those not near w_{PEO}*.

Blends outside w_{PEO}*. In Figure 6 we present cryo-TEM micrographs obtained from three premixed blends of OB9-4/OB9-12 at different mixing ratios. Neat dispersions of OB9-4 and OB9-12 form network[7] and spherical micelles, respectively. An equimolar mixture of these diblock copolymers self-assembles into short cylindrical micelles that coexist with spherical micelles (Figure 6A), qualitatively mimicking the intermediate morphology identified in Figure 2 between the constituent diblock copolymers. Increasing the OB9-4 content (2:1, Figure 6B) results in a decrease in the fraction of material that forms spherical micelles and the develop-

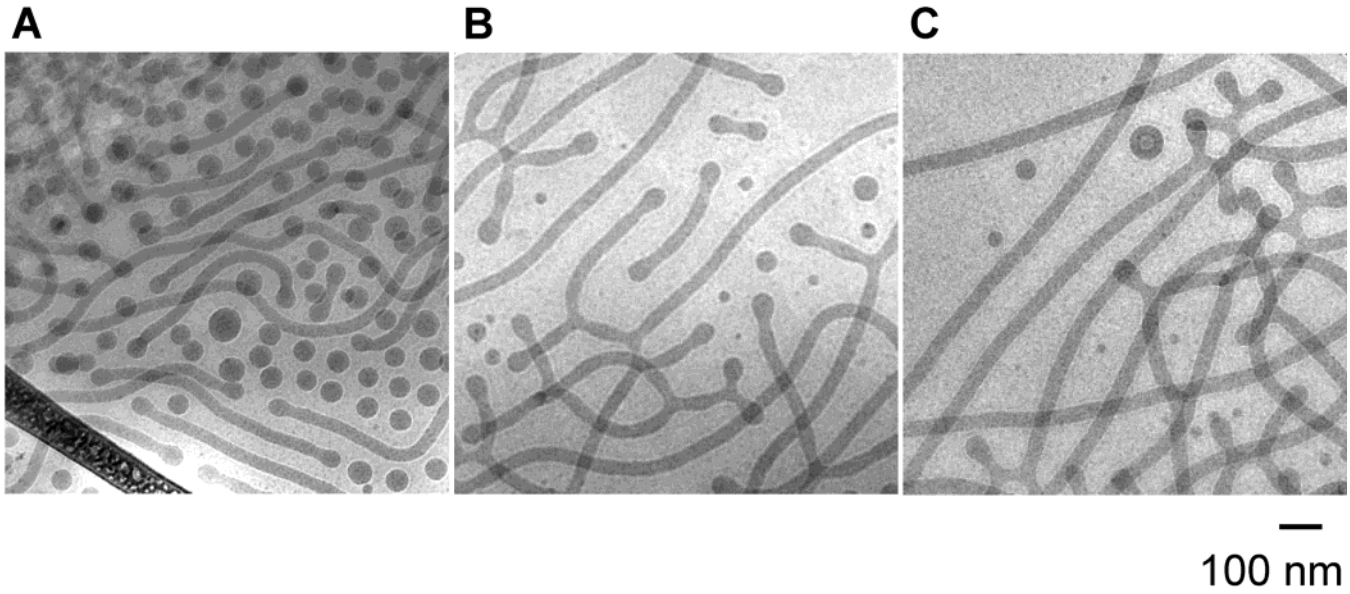

Figure 6. Cryo-TEM micrographs of premixed blends of OB9-4/OB9-12 with different molar mixing ratios: 1:1 (A), 2:1 (B), and 20:3 (C). The dominant morphology varies with the average composition of the blend.

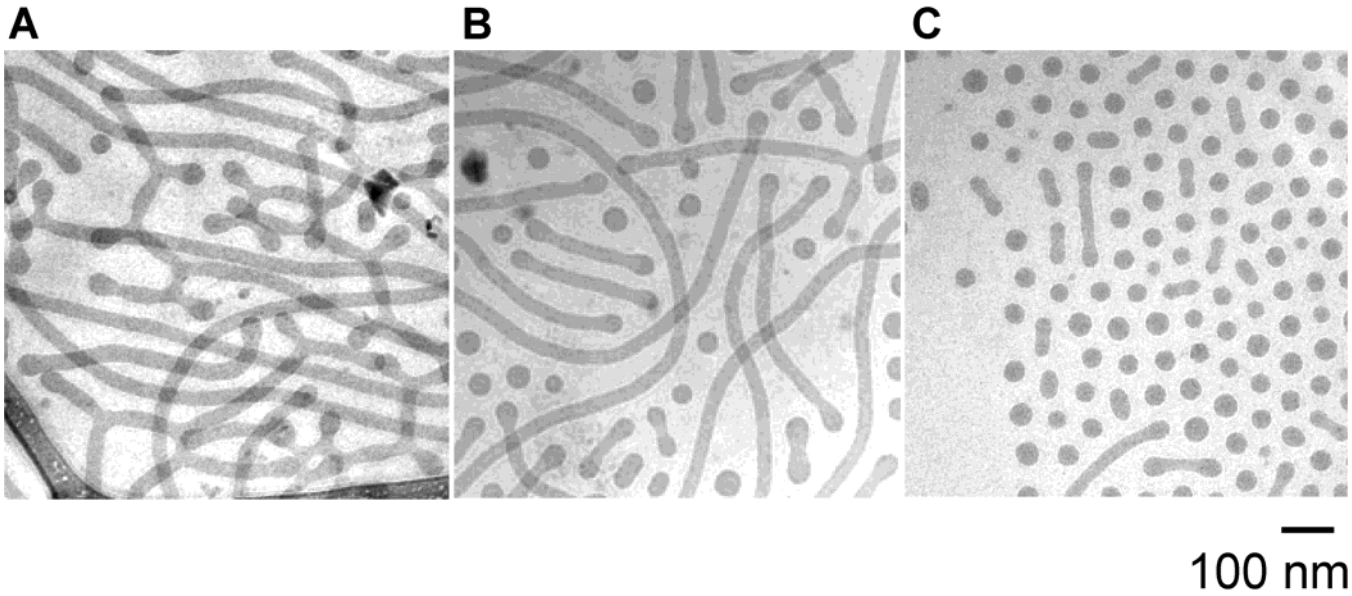

Figure 7. Cryo-TEM images obtained from premixed of blends of OB9-4 with OB1-5, OB1-3, and OB1-4 (A, B, and C, respectively). The morphology transitions from branched cylinders to cylinders to spherical micelles as the average hydrophilic content increases from $w_{PEO} = 0.38$ to 0.39 to 0.45.

ment of Y- junctions; some short cylindrical micelles were also documented as captured in this representative micrograph. Further increasing the OB9-4 content (20:3, Figure 6C) almost completely eliminates the spherical micelles coincident with the emergence of very long and branched cylindrical micelles, again consistent with a lower hydrophilic content. Micellar dimensions of the mixtures were found to be identical to those of the neat block copolymers.

Representative cryo-TEM images from dispersed mixtures of OB9-4 with three different OB1 series polymers (category B, Figure 3B) are presented in Figure 7. These images document the effects produced by mixing different low core molecular weight polymers (OB1-5, OB1-3, OB1-4) with a high core molecular weight diblock copolymer (OB9-4). The resultant mixtures capture the transition from branched cylindrical micelles exhibited by OB9-4/OB1-5 (Figure 7A) to short cylindrical micelles that coexist with spherical micelles formed by OB9-4/OB1-3 (Figure 7B) to spherical micelles with occasional short cylinders formed by OB9-4/OB1-4 (Figure 7C). Pure OB9-4 forms network structures while OB1-5, OB1-3, and OB1-4 form bilayers and cylinders (B + C), cylindrical micelles (C), and spherical micelles (S), respectively. Mixing higher core molecular weight diblock copolymer with a low core molecular weight diblock copolymer leads to the formation of micelles having core dimension intermediate to those associated with higher and lower core molecular weight diblock copolymers (see Table 3).

An unusual feature was documented in blends of OB9-1 and OB1-5 diblock copolymers (category B, Figure 3B). Premixed OB9-1/OB1-5 dispersions form long cylinders with some Y-junctions (Figure 8). A striking feature exhibited by these micelles is a pronounced undulation in the cylinder diameter near the terminus and at Y-junctions. Cylindrical micelles usually contain bulbous spherical end caps as is evident in

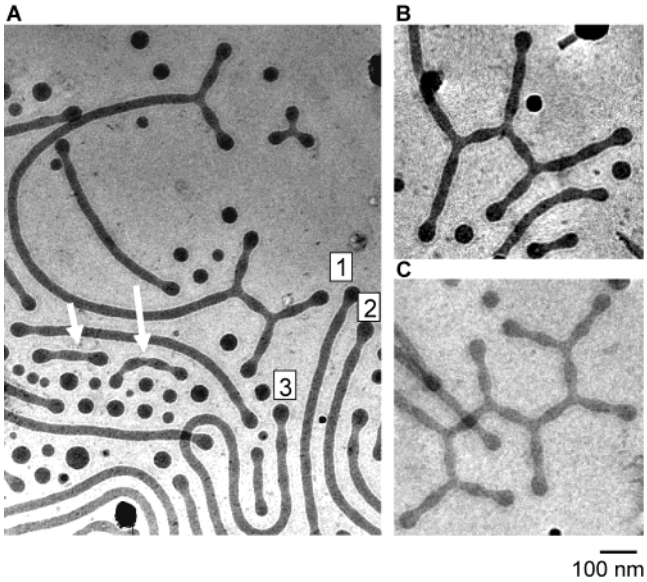

Figure 8. Cryo-TEM images from mixture OB9-1/OB1-5 depicting undulations and distended spherical end caps on wormlike cylindrical micelles. Short cylinders with an undulation (short arrow) and two undulations (long arrow) and cylinder ends with one, two, and three beads are marked correspondingly in (A). Panels B and C show branching with quantized undulations fixing the segment length between junctions. Two types of hyperbolic (saddle) surfaces characterize these morphologies (see Figure 13).

examples throughout this paper and elsewhere;[39] however, none are as conspicuous as those depicted in this blend. These beadlike deformations occur with a characteristic periodicity, which appears to be damped in the long central portions of the cylinders. Short cylinders with one and two beads can be seen in Figure 8A (short and long arrow, respectively). Cylinders with one, two, and three undulations are marked in Figure 8A. Figure 8B show branched portions of a cylindrical micelle with quantized undulations apparently dictating the arm lengths. Multiple undulating branches in Figure 8C highlight the localization of such features near the junctions and ends. These aggregates are stable, as heating the sample to 50 °C for a few days did not produce any noticeable change in the assembled morphologies. A comparison of OB9-1/OB1-3 shown in Figure 4B and OB9-1/OB1-5 presented in Figure 8 shows a transition from mainly spherical micelles to mainly cylindrical micelles over a very narrow composition range.

Blends around w_{PEO}*. Recently, we discovered network formation in aqueous dispersions of OB9-4 ($w_{PEO} = 0.34$ and $N_{PB} = 170$) (see Figure 9A). As a part of the present study, we attempted to mimic this network structure by blending OB9 diblock copolymers with greater ($w_{PEO} > 0.34$) and lesser ($w_{PEO} < 0.34$) compositions. For example, we blended equimolar mixtures of OB9-1 and OB9-6, resulting in an average composition of $\langle w_{PEO} = 0.34 \rangle$, identical to OB9-4. To our surprise this premixed blend self-assembles into a potpourri of delicate looking objects with bilayer, cylindrical, and complex junction structural elements, frequently mixed within individual moieties. These unusual structures are evident in all the cryo-TEM images taken from this mixture; Figure 9C displays many of the prevalent features. Perhaps the most striking is the octopus (or jelly fish)-like micelles, which are composed of a flat bilayer with protruding cylindrical micelles along the edges. These octopus-like entities are common, although they occur with a variable number of cylindrical arms. Several examples are shown in Figure 10 containing 4, 5, 6, 7, 8, 9, 10, and 14 arms attached to the flat central portion. In all these octopus-like aggregates the cylindrical arms are symmetrically distributed along the circumference of the central flat bilayer as is evident in Figures 9C and 10. Occasionally, these objects appear to be folded on a side with the cylindrical arms protruding from a hemispherical bilayer cap. Obviously, the confinement created by the

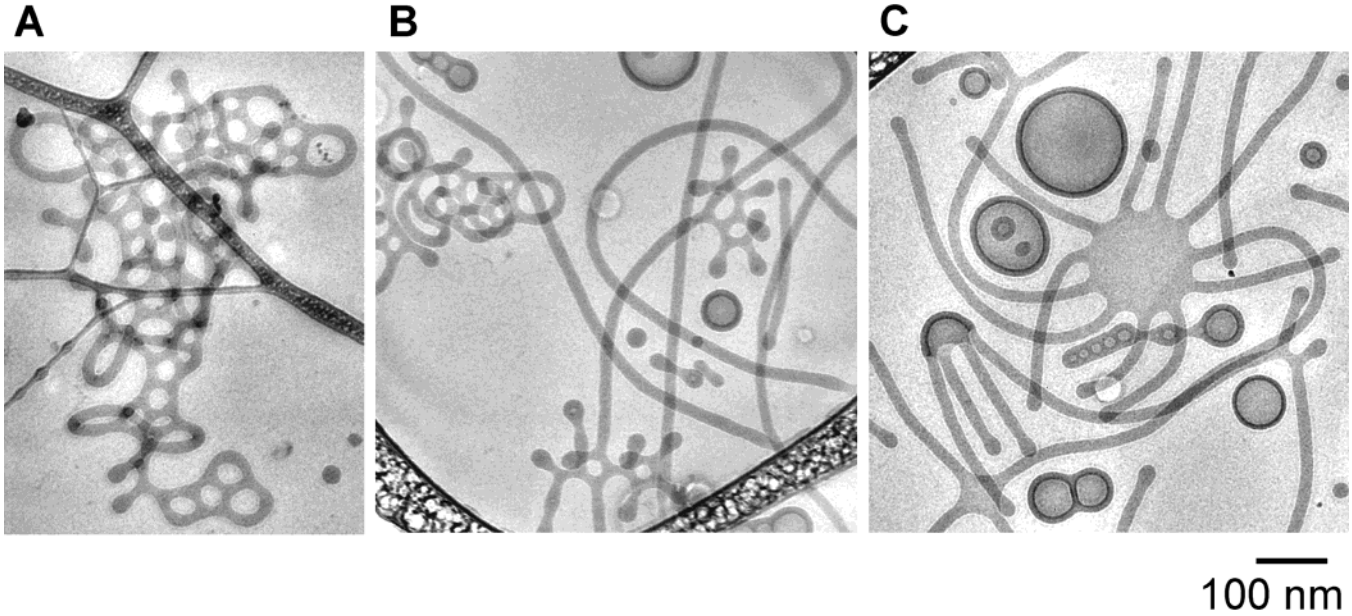

Figure 9. Cryo-TEM micrographs from three dispersions with identical compositions, $\langle w_{PEO} = 0.34 \rangle$; the molecular weight distribution broadens from A to B to C. (A) A network fragment from OB9-4, a single component dispersion. This picture is reproduced from ref 7. (B) Blend OB9-11/OB9-15. A bimodal distribution of component compositions ($w_{PEO} = 0.39$ and 0.30) breaks the network. (C) A broader distribtion ($w_{PEO} = 0.24$ and 0.42, OB9-6/OB9-1) produces a variety of morphologies including vesicles, wormlike micelles, and a new type of hybrid particle referred to as an octopus. Two of these objects, comprised of cylindrical arms radiating from a single bilayer, are evident in this image, one with 11 and one with 4 arms.

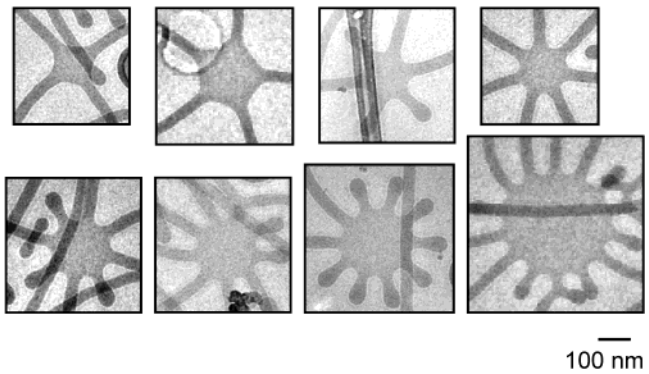

Figure 10. A collection of cryo-TEM images obtained from the OB9-1/OB9-6 blend, documenting octopi with different arm numbers. In each case the arms are uniformly distributed around the periphery of the bilayer, creating a new type of hyperbolic surface (see Figure 13).

thin-film (cryo-TEM) environment (200−300 nm thick) will limit the full spectrum of three-dimensional configurations available to such structures. We speculate as to the origins of these octopus-like assemblages in the Discussion section.

A second blend of diblock copolymer near w_{PEO}* was created from OB9-11 and OB9-15, which also occur on either side of the network but with half the spread in w_{PEO} as for the previous system. OB9-11 forms long, branched cylindrical micelles while OB9-15 produces a coexistence of bilayers and branched cylinders. The average composition of the blend was $\langle w_{PEO} = 0.34 \rangle$, identical to the OB9-1/OB9-6 blend and the network forming block copolymer. Table 2 lists the polydispersity indices for the PEO blocks in these mixtures. Micellar morphologies exhibited by this blend are qualitatively distinct from the OB9-1/OB9-6 blend, devoid of any octopus-like structures (see Figure 9B). This blend more closely mimics the network morphology although it does not phase separate like pure OB9-4. Another blend of OB9-1/OB9-6 diblock copolymers having an average composition of $\langle w_{PEO} = 0.37 \rangle$ (Table 2) displays micellar morphologies (not shown) very similar to those found in the OB9-11/OB9-15 blend.

Discussion

The results presented in Figures 4−10 firmly establish that the micelle morphologies assumed by diblock copolymers are highly path dependent. Cryo-TEM captures this path dependence in a unique way, directly imaging the associated complex morphological structures. In contrast, scattering methods such as SAXS and SANS produce data that reflect ensemble averages over all particle shapes and sizes, which can obscure essential structural details.

At equilibrium there must be a dynamic exchange of polymers between micelles, a condition not satisfied by any of the aqueous dispersions reported here. Even after several months postmixed solutions exhibited two distinct morphological populations (see Figures 4A and 5A). We assume the premixed solutions are similarly constrained. These findings corroborate our previous SANS experiments,[6] and in light of both studies, it seems reasonable to expect that the exchange times leading to micelle equilibration can be extraordinarily long, perhaps many years.

This lack of chain exchange (or extremely slow exchange kinetics) hampers establishment of global

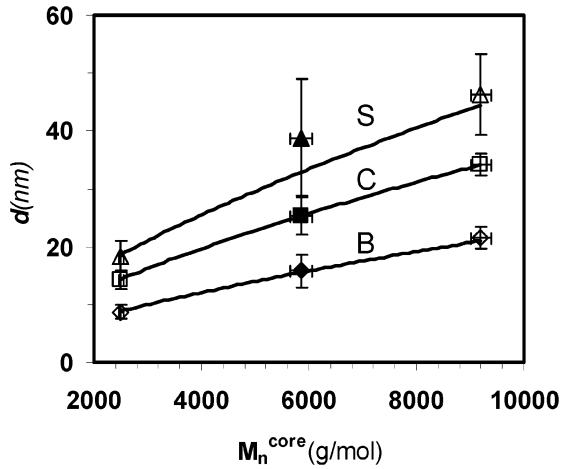

Figure 11. Dimension d (diameter or thickness) as a function of core block number-average molecular weight (M_n^{core}) for spherical (S) (▲), cylindrical (C) (■), and bilayer (B) (◆) micelles. The curves identify the scaling exponents of $^2/_3$.

equilibrium and places severe constraints on structural evolution. The most important factor controlling diblock copolymer exchange between micelles is the solubility of individual polymer chains in water, which is typically expressed in terms of the critical micelle concentration (cmc). Cmc values for diblock copolymer micelles may be much lower than those for analogous low molecular weight surfactants[40] as the cmc decreases exponentially with increasing core block length.[41] Various exchange mechanisms[22,42] have been proposed for micelle equilibration in amphiphilic systems, but our results suggest that the high degree of amphiphilicity prevents any of these from being operative. The residence time of chains in a micelle is governed by the free energy of micellization;[23] literature estimates for the standard free energies of hydrocarbon and PEO micellization are $\Delta G_m(-CH_2-) = -0.68$ kcal/mol and $\Delta G_m(-CH_2-CH_2-O-) = 0.19$ kcal/mol at 25 °C,[41] respectively. These estimates suggest that the residence times for block copolymers used in this study, for example, OB9-1 containing 680 methylene and 150 ethylene oxide units, must be very large. Halperin and Alexander[43] pointed out that the escape and reentry of unimer chains in block copolymer micellar aggregates may be kinetically hindered or fully frozen because the free energy of fission or fusion is often too high.

In the remainder of this discussion we consider three distinct aspects of our experimental results: nonergodicity and the morphologies recorded for blends outside and near w_{PEO}*.

Nonergodicity. A prominent feature in Figures 4 and 5 is the difference in core dimensions obtained from different blends. The disparity in micellar sizes results from differences in the core block molecular weight, which is different for the two series of diblock copolymers studied. A plot of micellar sizes, determined from numerous micrographs, against core molecular weight is shown in Figure 11 for pure (open symbols) and blended (filled symbols) block copolymers. For each of the three morphologies (B, C, and S) the core dimension scales with the core molecular weight with an exponent of $^2/_3$ (solid curves), in agreement with strong segregation theory[44,45] based on the interplay between chain entropy and interfacial tension. Thus, we conclude that the premixed micelles contain diblock copolymer that is distributed uniformly across all the micelles.

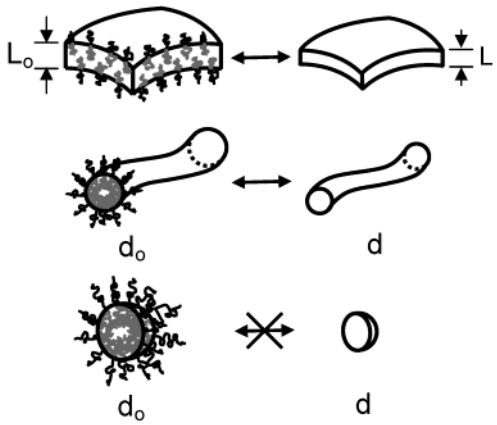

Figure 12. Illustration showing allowed and disallowed structural adjustments for different micelle geometries. Vesicles (bilayers) and cylinders can make dimensional adjustments by increasing or decreasing chain stretching with simultaneous retraction in length, thereby optimizing the local free energy. This mechanism is not available to spherical micelles.

A careful assessment of Figure 11 and Table 3 reveals a small but statistically significant difference in the standard deviation in core dimensions between the spheres and cylinders and bilayers. This variation is particularly evident in the higher molecular weight micelles, where a 15% spread in sphere diameters compares with 6% for the cylinders and 9% for the bilayers. We believe these differences reflect variations in local equilibration. As illustrated in Figure 12, once formed nonergodic zero-dimensional spheres (S) have no mechanism for adjusting the micelle diameter. On the other hand, one-dimensional cylinders can easily shorten and fatten, or vice versa, thereby adjusting the degree of core chain stretching balanced against interfacial tension. Bilayer vesicles, two-dimensional sheets folded into zero-dimensional objects, are more constrained than cylinders but less so than spheres. A vesicle can change diameter spontaneously, but only if water is transported into or out of the center by diffusion through the bilayer membrane. The binary blends also exhibit a slightly greater distribution of core dimensions than the pure components, again most evident with the spheres, where a 26% standard deviation in diameters was recorded. This effect is visible in Figures 6A, 7C, and 8A.

These results lead to the inescapable conclusion that the block copolymer micelles exist in kinetically frozen states. This may explain the prevalence of multiple morphologies as evidenced by the broad morphology windows (B + C and C + S) found in Figure 2 and their general absence in most surfactant[46] solutions. In conventional surfactants free movement of molecules between micelles facilitates global equilibration, which should eliminate coexistence windows in monodisperse systems. Coexistence of morphologies in polymeric systems has been attributed to the glassy nature of the core block[25] and diblock copolymer polydispersity;[36] neither of these is likely to affect our results. Except near the network forming condition (see below), our imposition of bimodality in the premixed blends did not qualitatively affect the distribution of micelle types; however, binary blending does appear to shift the morphology windows somewhat (see below).

We believe the principal reason for the occurrence of the wide coexistence windows is nonergodicity. This deduction also suggests that coalescence of particles, for example spheres with spheres or cylinders, is inoperative as well. On the other hand, we do not expect formation of spheres from cylinders to be restricted in the same way. Also, we anticipate facile intramicelle transitions provided they do not involve a change in topology, such as formation of a Y-junction by the creation of a spherical end cap on a cylinder.

Blends outside w_{PEO}*. The images presented in Figure 6 illustrate morphologies associated with a single core block ($N_{PB} = 170$) and a binary mixture of corona blocks (category A, Figure 3). These cryo-TEM micrographs show morphological transitions as the composition of the blend (and/or polydispersity in hydrophilic block lengths, Table 2) is varied. The presence of cylindrical micelles in a mixture containing polymers that do not form cylinders individually is indicative of bulk mixing of both polymer chains within the aggregates. Milner and Witten[47] proposed that mixtures of homologous block copolymers with different molecular weight and modest compositional asymmetry should resist segregation consistent with these results. Prior studies dealing with diblock copolymer dispersions have overlooked the impact of blending on micelle morphologies concentrating instead on properties such as the cmc, aggregation number, and micelle sizes.[17,48]

Figure 7 displays representative images of dispersions obtained from three premixed blends containing OB9-4 mixed with OB1-5, OB1-3, and OB1-4 (category B, Figure 3). Here again premixing leads to a single relatively monodisperse set of micelle dimensions that exhibit transitions from branched cylinders, to cylinders and spheres, to nearly all spheres as $\langle w_{PEO} \rangle$ ranges from 0.38 to 0.45. However, these blend results do not conform to the morphology diagram developed for the single components (Figure 2). For example, the equimolar mixture of OB9-4 and OB1-4 ($\langle w_{PEO} \rangle = 0.45$) is dominated by spherical micelles while a single component $N_{PB} = 109$, $w_{PEO} = 0.45$ dispersion is anticipated to form only cylindrical micelles. Obviously, the core and corona packing constraints are affected by the molecular weight and composition distributions. This may be due to an effective attractive interaction between different length core blocks. A combination of short and long chains can result in a net reduction in stretching free energy, a form of nonideal mixing that would disrupt application of simple mixing rules.[49]

The phase diagram associated with mixtures of surfactants has been shown to be different than that measured for a single component.[50] Mixing copolymers having identical core blocks preserves the micelle size (Figure 3A,C) while these dimensions can be tailored by mixing copolymers having different core blocks (Figure 3B) as discussed earlier. In both cases the corona (PEO) block distribution in chain lengths is affected, although this does not appear to have a significant effect on the micelles.

Perhaps the most provocative images presented in this study are found in Figure 8. These branched and undulating wormlike micelles were obtained by mixing equal amounts of OB9-1 and OB1-5, homologous diblocks, each with $w_{PEO} = 0.42$. This composition places this mixture at the transition between cylinders and spheres based on the series of results shown in Figure 7. And although bulbous spherical end caps typically are encountered at the terminus of the PEO−PB cylindrical micelles, we believe the combination of increasing molecular weight and polydispersity create a particular

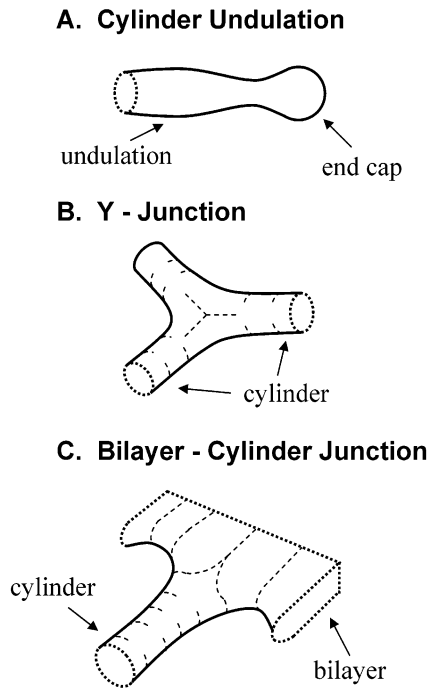

Figure 13. Structural elements with hyperbolic (saddle) surfaces identified in this work. (A) Spherical end cap and associated undulations in a cylindrical micelles. The magnitude of the oscillation in diameter appears to be magnified by blending low and high molecular weight diblock copolymers. (B) Y-junction that connects cylindrical micelles. This element combines bilayerlike and cylindrical curvatures and appears to be favored with increasing diblock copolymer molecular weight and compositions intermediate to vesicles and wormlike micelles. (C) The structural element characterizing the octopus morphology is a transition from a bilayer to a cylinder, created by intramicelle segregation of B and C forming diblock copolymers.

sensitivity to undulations that resemble the well-known Rayleigh instability, a peristaltic mode of deformation encountered with liquid filaments and jets of fluid.[51] However, whereas the Rayleigh instability generally is mediated by dynamical events, we will argue that the micelle undulations are locally equilibrated static features. By "locally equilibrated" we mean that an individual micelle or piece of micelle has attained a preferred dimension, e.g., cylinder diameter, branch structure, undulation period and amplitude, or vesicle wall thickness.

The stability of cylindrical surfaces depends mainly on the curvature energy governed by the spontaneous radius of curvature and the bending energy.[52] Safran[53] showed that the free energy of a cylinder with undulations of wavelength greater than a critical value is lower than that of a perfect cylinder. These undulations eventually transform into a pearl-shaped Rayleigh-like instabilities leading to cylindrical breakup into spheres having a lower surface-to-volume ratio. The chain packing perturbation created by a cylinder terminus, a combination of a hemisphere and cylinder, is well-known to produce a zone of negative Gauss curvature (saddle surface) at the junction between these two geometries (see Figure 13A).[39] However, to the best of our knowledge, in surfactants this single undulation quickly damps as the cylindrical morphology is established. We also have identified this type of structure in PEO−PB micelles as described in previous reports.[36]

The undulations found in Figure 8 are remarkable for two reasons. First, they propagate with a fixed wavelength for as many as three periods away from the spherical terminus. Second, localization at the end of cylindrical micelles is correlated with branch formation and even appears to control the branch length. We are unaware of any reports demonstrating this level of structural organization in block copolymers or surfactants. Apparently, mixing two different, but compositionally equivalent, diblocks enhances this type of undulation. A complete description of this effect is outside the scope of this publication. Here we offer a few observations and deductions leaving a more complete treatment to the future.

Clearly, the undulations are correlated with the occurrence of highly inflated spherical end caps. Quantitative measurements indicate the cap diameter is roughly 66% greater than the associated cylinder diameter. (Here we note that these measurements were conducted on individual micelles like the one shown in Figure 8A, which contains both an unperturbed cylindrical section and branches with spherical caps on both ends. On the basis of previous arguments, we believe such micelles are locally equilibrated.) This disparity is even greater than the ratio of sphere to cylinder diameters identified in Table 3, which range from 1.29 ($N_{PB} = 46$) to 1.35 ($N_{PB} = 170$) for the pure components and 1.53 for the $\langle N_{PB} \rangle = 109$ mixtures. Moreover, at the narrowest portion of the undulations the diameter is just 70% of the uniform cylinder dimension. We believe this variation in domain diameter is exacerbated by the presence of two diblock molecular weights, facilitating end-cap dilation and the subsequent constriction as illustrated in Figure 13.

These undulations have a distinct preferred period along with a proclivity to spawn branches. The net effect is quantized arm lengths, most frequently containing one undulation and a spherical end cap, although examples with two undulations are also found in Figure 8B. A complete understanding of the molecular factors responsible for this phenomenon will require a proper theoretical treatment.

Blends around w_{PEO}*. Evidence of yet greater intramicelle segregation was produced at a blend composition, $\langle w_{PEO} \rangle = 0.34$, coincident with the formation of a network[7] in the monomodal and nearly monodisperse sample OB9-4. Figure 9A is a cryo-TEM image of a network fragment from OB9-4, reproduced from ref 7. After a few days at room temperature a 1% solution of this polymer phase separates into a dense network phase located above pure water. Blending destroys the network as illustrated in Figure 9B,C. The broadest spread in composition, $w_{PEO} = 0.24$ (OB9-6) and $w_{PEO} = 0.42$ (OB9-1), leads to a complex yet fascinating array of morphological objects as revealed in Figure 9C. Consistent with the other examples, this specimen produces a mixture of dispersed objects, including vesicles, linear and branched wormlike micelles, and numerous hybrid particles that we collectively refer to as "octopus-like". The defining feature of the octopus is a central sheet with radiating cylindrical arms symmetrically distributed along the periphery. This structural motif is quite common in this mixture, although with variable arm functionality (see Figure 10).

We have identified the piece at the center of the octopus as a single bilayer sheet based on simulated TEM images as sketched in Figure 14. A single bilayer projects a distinctly different image than a vesicle. The central portion of the former appears to be lighter, and

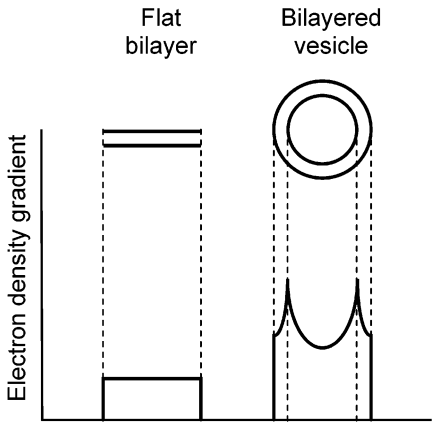

Figure 14. Schematic illustration of the cryo-TEM images projected from electron density profiles associated with a flat bilayer, which forms the central portion of the octopus morphology, and spherical bilayer vesicles.

the edges are devoid of the dark fringe apparent on the inside edge of the vesicle wall. This feature is evident in several vesicles present in Figure 9C, and in the four-arm octopus folded on its side, where the hemispherical cupped bilayer mimics a half-vesicle. The cylindrical arms also are somewhat darker than the central bilayer as would be expected on the basis of the dimensions listed in Table 3.

Narrowing the spread in compositions, $w_{PEO} = 0.30$ (OB9-15) and $w_{PEO} = 0.39$ (OB9-11), (Figure 9B) eliminates the occurrence of the octopus morphology and increases the degree of (short) cylinder branching, which coexists with numerous long cylindrical micelles and a minority population of vesicles.

We interpret the octopus morphology as a state of intramicellar segregation, driven solely by a bimodal distribution of PEO corona block molecular weights which leads to two distinct interfacial curvatures. The constituent diblock copolymers individually tend to form bilayers (vesicles) and wormlike micelles. Assuming these polymers mix in the undiluted melt state,[2−4] they would initially be driven into a uniform dispersion, possibly mimicking the highly branched morphology displayed by OB9-4; recall this mixture has a single core molecular weight. Molecular diffusion along these nonergodic micelles (facilitated by the low T_g of the core forming block) would provide a mechanism for local segregation, transforming branched saddle surfaces into cylindrical and bilayer segments rich in OB9-1 and OB9-6, respectively. Figure 15 illustrates a hyperbranched cylindrical micelle that appears to be consolidating Y-junctions in just this manner. (Notice the less prominent spherical end caps and undulations on these cylinders.) Consistent with our earlier conclusion regarding structural transformations, these internally segregated micelles seem to resist fracturing into separate C and B micelles. Instead, surface tension at the edge of the flat bilayer is minimized by symmetric placement of the cylindrical arms (see Figure 10). We suspect that the formation of octopus micelles from vesicles is inhibited by the requisite topological transformation, i.e., an unfavorable transition from a closed spherical vesicle devoid of edges to a bilayer sheet with bilayer−cylinder junctions.

Halperin[54] anticipated this result 15 years ago when he proposed that binary micelles could undergo microphase separation via two mechanisms—intramicellar and intermicellar segregation—depending on chain mobility. We believe our system of diblock copolymers provides the first clear verification of Halperin's hypothesis.

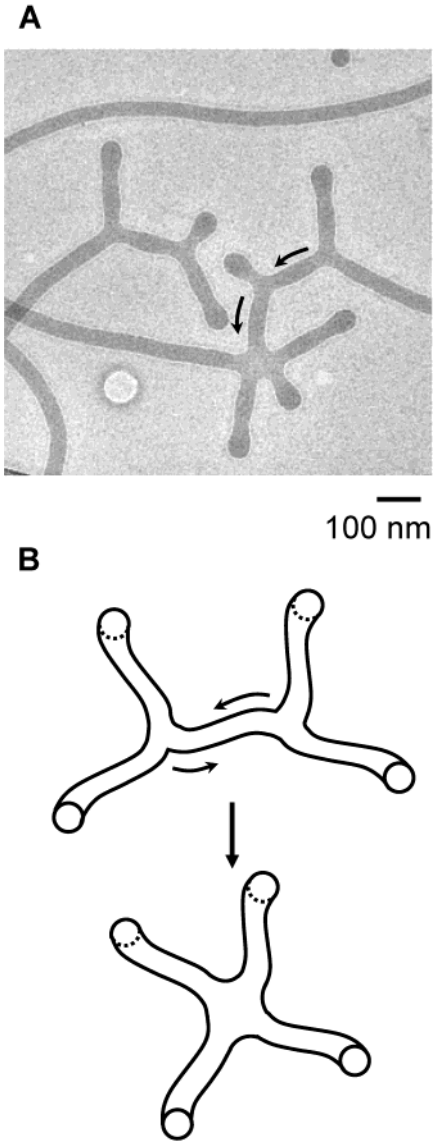

Figure 15. (A) Cryo-TEM micrograph of OB9-1/OB9-6 blend micelles. The five-arm junction may evidence the initial stages of octopus morphology formation. Transport of diblock copolymer molecules along the cylindrical portions of the micelle would permit evolution of a connected bilayer sheet as indicated in (B).

From these results we conclude that the network structures, and individual Y-junctions, reflect some degree of packing frustration, representing a compromise between the bilayer and cylindrical geometries (see Figure 13). In fact, others have made this point in dealing with oil/water/surfactant systems.[55] A single component dispersion must accommodate this packing dilemma, and apparently increasing molecular weight facilitates this process (Figure 2). However, the binary blend has an added degree of freedom, which is exercised in the form of the octopus morphology, thereby minimizing the number of Y-junctions while creating a new type of saddle surface. Thus, three distinct structures containing negative Gauss curvature (i.e., hyperbolic interfaces[56]) are now established in the PEO−PB block copolymer micellar dispersions (see Figure 13). (We should point out that Eisenberg and co-workers[19,57−60] have identified a plethora of structures,

containing a myriad of complex shapes and topologies, in a variety of other block copolymer dispersions.) We hope that the images provided here will motivate fresh theoretical activity that may aid in understanding these phenomena.

Finally, we summarize the assortment of interfacial surfaces now documented in PEO−PB diblock copolymer aqueous dispersions. The three classical morphologies, spheres, cylinders, and bilayers, are characterized by elliptic and parabolic surfaces, each with mean and Gaussian curvatures that are greater than or equal to zero. Three hyperbolic surfaces[56] also have been identified as illustrated in Figure 13, characterized by negative Gaussian curvature, which favorably reduces the curvature elastic energy. Morphological forms exhibiting hyperbolic surfaces like undulations in cylinders and octopus-like structures result as a consequence of polymer segregation within a micelle. A detailed assessment of the roles of block molecular weight and modality is beyond the scope of this article. However, our findings reinforce the notion that block copolymer amphiphiles offer a rich and quantifiable complexity of packing geometries[7,61,62] not readily available with low molecular weight systems.

Summary

This report deals with two issues related to micelle formation in aqueous dispersions of nonionic block copolymer amphiphiles: nonergodicity and morphology in binary mixtures. By comparing the cryo-TEM images from premixed and postmixed blends, we have shown that macromolecular surfactants form isolated micelles that do not exchange polymers over extended periods of time, well beyond the normal experimental time frame. This failure to globally equilibrate, referred to as nonergodicity, has profound consequences on the distribution of morphologies found in PEO−PB-based dispersions. These effects are evident at molecular weights of just 2000 Da.

Premixing block copolymers with different molecular weights and compositions leads to intermediate micelle dimensions that are well approximated by strong segregation scaling theory. However, at compositions that favor cylindrical branching and network formation in the monomodal materials, blending may produce enhanced cylindrical undulations coupled with branch formation and distended spherical end caps and intramicellar chain segregation leading to mixed structures containing single bilayer sheets with radiating cylindrical micelles. These structures have been considered within the constraints of nonergodicity and contrasted with conventional low molecular weight surfactants. We hope to exploit these phenomena in developing self-assembled block copolymer dispersions for a variety of applications including as scaffolding for the growth of artificial tissue.

Acknowledgment. The authors thank R. Strey (Germany) and D. C. Morse (Minnesota) for helpful discussions and Mitchell H. E. Dyrdahl for help with the polymer synthesis. Financial support for this research was provided by the NIH (1R21EB00989-01) and by the Materials Research Science and Engineering Center (MRSEC) at the University of Minnesota.

References and Notes

(1) Shiloach, A.; Blankschtein, D. *Langmuir* **1998**, *14*, 1618−1636.
(2) Shi, A.-C.; Noolandi, J. *Macromolecules* **1995**, *28*, 3103−3109.
(3) Zhao, J.; Majumdar, B.; Schulz, M. F.; Bates, F. S.; Almdal, K.; Mortensen, K.; Hajduk, D. A.; Gruner, S. M. *Macromolecules* **1996**, *29*, 1204−1215.
(4) Court, F.; Hashimoto, T. *Macromolecules* **2002**, *35*, 2566−2575.
(5) Alexandridis, P., Lindman, B., Eds. *Amphiphilic Block Copolymers: Self-Assembly and Applications*; Elsevier: Amsterdam, 2000.
(6) Won, Y. Y.; Davis, H. T.; Bates, F. S. *Macromolecules* **2003**, *36*, 953−955.
(7) Jain, S.; Bates, F. S. *Science* **2003**, *300*, 460−464.
(8) Zana, R. In *Amphiphilic Block Copolymers: Self-Assembly and Applications*; Alexandridis, P., Lindman, B., Eds.; Elsevier: Amsterdam, 2000; pp 221−252.
(9) Wang, Y.; Kausch, C. M.; Chun, M.; Quirk, R. P.; Mattice, W. L. *Macromolecules* **1995**, *28*, 904−911.
(10) Liu, G. *Can. J. Chem.* **1995**, *73*, 1995−2003.
(11) Rager, T.; Meyer, W. H.; Wegner, G.; Winnik, M. A. *Macromolecules* **1997**, *30*, 4911−4919.
(12) Hecht, E.; Hoffmann, H. *Colloids Surf., A* **1995**, *96*, 181−197.
(13) Honda, C.; Abe, Y.; Nose, T. *Macromolecules* **1996**, *29*, 6778−6785.
(14) Honda, C.; Hasegawa, Y.; Hirunuma, R.; Nose, T. *Macromolecules* **1994**, *27*, 7660−7668.
(15) Michels, B.; Waton, G.; Zana, R. *Langmuir* **1997**, *13*, 3111−3118.
(16) Fleischer, G. *J. Phys. Chem.* **1993**, *97*, 517−521.
(17) Creutz, S.; van Stam, J.; Antoun, S.; De Schryver, F. C.; Jerome, R. *Macromolecules* **1997**, *30*, 4078−4083.
(18) Munk, P.; Ramireddy, C.; Tian, M.; Webber, S. E.; Prochazka, K.; Tuzar, Z. *Makromol. Chem., Macromol. Symp.* **1992**, *58*, 195−199.
(19) Zhang, L.; Eisenberg, A. *Science* **1995**, *268*, 1728−1731.
(20) Rager, T.; Meyer, W. H.; Wegner, G. *Macromol. Chem. Phys.* **1999**, *200*, 1672−1680.
(21) Dormidontova, E. E. *Macromolecules* **1999**, *32*, 7630−7644.
(22) Aniansson, E. A. G.; Wall, S. N. *J. Phys. Chem.* **1974**, *78*, 1024−1030.
(23) Aniansson, E. A. G.; Wall, S. N.; Almgren, M.; Hoffmann, H.; Kielmann, I.; Ulbricht, W.; Zana, R.; Lang, J.; Tondre, C. *J. Phys. Chem.* **1976**, *80*, 905−922.
(24) Schillen, K.; Yekta, A.; Ni, S.; Winnik, M. A. *Macromolecules* **1998**, *31*, 210−212.
(25) Yu, Y.; Zhang, L.; Eisenberg, A. *Langmuir* **1997**, *13*, 2578−2581.
(26) Willner, L.; Poppe, A.; Allgaier, J.; Monkenbusch, M.; Richter, D. *Europhys. Lett.* **2001**, *55*, 667−673.
(27) Gao, Z.; Eisenberg, A. *Macromolecules* **1993**, *26*, 7353−7360.
(28) Linse, P. *Macromolecules* **1994**, *27*, 6404−6417.
(29) Terreau, O.; Luo, L.; Eisenberg, A. *Langmuir* **2003**, *19*, 5601−5607.
(30) Halperin, A.; Tirrell, M.; Lodge, T. P. *Adv. Polym. Sci.* **1992**, *100*, 31−71.
(31) Hillmyer, M. A.; Bates, F. S. *Macromolecules* **1996**, *29*, 6994−7002.
(32) Ferry, J. D. *Viscoelastic Properties of Polymers*, 3rd ed.; Wiley: New York, 1980.
(33) Lysenko, E. A.; Bronich, T. K.; Slonkina, E. V.; Eisenberg, A.; Kabanov, V. A.; Kabanov, A. V. *Macromolecules* **2002**, *35*, 6351−6361.
(34) Bellare, J. R. In *CEMS*; University of Minnesota: Minneapolis, 1988.
(35) Talmon, Y. *Ber. Bunsen-Ges.* **1996**, *100*, 364−372.
(36) Won, Y.-Y.; Brannan, A. K.; Davis, H. T.; Bates, F. S. *J. Phys. Chem. B* **2002**, *106*, 3354−3364.
(37) Shen, H.; Eisenberg, A. *J. Phys. Chem. B* **1999**, *103*, 9473−9487.
(38) Israelachvili, J. *Intermolecular and Surface Forces*, 2nd ed.; Academic Press: San Diego, 1992.
(39) Tlusty, T.; Safran, S. A. *J. Phys.: Condens. Matter* **2000**, *12*, A253−A262.
(40) Zhao, C. L.; Winnik, M. A.; Riess, G.; Croucher, M. D. *Langmuir* **1990**, *6*, 514−516.
(41) Schick, M. J., Ed. *Surfactant Science Series, Vol. 23: Nonionic Surfactants: Physical Chemistry*; Marcel Dekker: New York, 1987.
(42) Kahlweit, M. *J. Colloid Interface Sci.* **1982**, *90*, 92−99.
(43) Halperin, A.; Alexander, S. *Macromolecules* **1989**, *22*, 2403−2412.

(44) De Gennes, P. G. *J. Polym. Sci., Polym. Phys. Ed.* **1978**, *16*, 1883−1885.
(45) Bates, F. S.; Fredrickson, G. H. *Phys. Today* **1999**, *52*, 32−38.
(46) Ben-Shaul, A.; Gelbart, W. M. In *Micelles, Membranes, Microemulsions and Monolayers*; Gelbart, W. M., Ben-Shaul, A., Roux, D., Eds.; Springer-Verlag: New York, 1994; pp 1−104.
(47) Milner, S. T.; Witten, T. A. *J. Phys. (Paris)* **1988**, *49*, 1951−1962.
(48) Sens, P.; Marques, C. M.; Joanny, J. F. *Macromolecules* **1996**, *29*, 4880−4890.
(49) Dan, N.; Safran, S. A. *Macromolecules* **1994**, *27*, 5766−5772.
(50) Kaler, E. W.; Herrington, K. L.; Miller, D. D.; Zasadzinski, J. A. N. *NATO ASI Ser., Ser. C: Math. Phys. Sci.* **1992**, *369*, 571−577.
(51) Granek, R. *Langmuir* **1996**, *12*, 5022−5027.
(52) Safran, S. A. *Surf. Sci.* **2002**, *500*, 127−146.
(53) Safran, S. A., Ed. *Statistical Thermodynamica of Surfaces, Interfaces, and Membranes*; Addison-Wesley: New York, 1994.
(54) Halperin, A. *J. Phys. (Paris)* **1988**, *49*, 131−137.
(55) May, S.; Bohbot, Y.; Ben-Shaul, A. *J. Phys. Chem. B* **1997**, *101*, 8648−8657.
(56) Seddon, J. M. *Biochim. Biophys. Acta* **1990**, *1031*, 1−69.
(57) Yu, K.; Zhang, L.; Eisenberg, A. *Langmuir* **1996**, *12*, 5980−5984.
(58) Yu, Y.; Zhang, L.; Eisenberg, A. *Macromolecules* **1998**, *31*, 1144−1154.
(59) Yu, G.-e.; Eisenberg, A. *Macromolecules* **1998**, *31*, 5546−5549.
(60) Shen, H.; Eisenberg, A. *Macromolecules* **2000**, *33*, 2561−2572.
(61) Yu, K.; Eisenberg, A. *Macromolecules* **1996**, *29*, 6359−6361.
(62) Burke, S.; Eisenberg, A. *Polymer* **2001**, *42*, 9111.

MA035467J